Experimental verification of Pyragas-Schöll-Fiedler control

Clemens von Loewenich and Hartmut Benner

Institute for Solid State Physics, Darmstadt University of Technology,

Hochschulstraße 6, D-64289 Darmstadt, Germany

Wolfram Just

Queen Mary University of London, School of Mathematical Sciences,

Mile End Road, London E1 4NS, UK

(Dated: 17th August 2010)

Abstract

We present, for the first time to our best knowledge, an experimental realisation of time-delayed feedback control proposed by Schöll and Fiedler. The scheme enables us to stabilise torsion-free periodic orbits in autonomous systems, and to overcome the so-called odd number limitation. The experimental control performance is in quantitative agreement with the bifurcation analysis of simple model systems. The results uncover some general features of the control scheme which are deemed to be relevant for a large class of setups.

PACS numbers: 05.45.Gg, 02.30.Ks, 07.05.Dz

Keywords: Control of chaos, time-delay dynamics, electronic circuit experiment, bifurcation analysis

I. INTRODUCTION

Using time delayed feedback for the purpose of stabilising periodic target states in complex dynamical systems, as introduced about two decades ago by Pyragas [1], is still one of the most active branches in applied dynamical systems theory (cf., e.g., [2] for a recent comprehensive overview). To some extent the appeal of such a topic comes from the observation that time-delayed feedback control is just one of the simplest experimentally relevant setups for studying time delay dynamics in general, and aspects of synchronisation in particular (cf., e.g., [3]). Unfortunately, like for most subjects of experimental relevance, there are known only a few general properties of time delayed feedback control. It was believed for more than one decade that time delayed feedback control suffers from the so-called odd number limitation [4], i.e., only orbits of a particular type can be stabilised. It has been shown recently by Fiedler et al. [5] that such a statement uses a crucial hidden assumption, and that in autonomous systems any periodic state should be accessible for time-delayed feedback control. The authors of Ref.[5] investigated the Hopf normal form as a paradigmatic model system. In addition, a particularly successful coupling scheme of the control force was proposed. In mathematical terms the model can be written as

$$\dot{z} = (\lambda + i)z(t) + (1 + i\gamma)|z(t)|^2 z(t) - K(z(t) - z(t - \tau)) \,. \tag{1}$$

Here $z(t) \in \mathbb{C}$ denotes the two dimensional state variable, $z(t) - z(t-\tau)$ the time-delayed feedback, and $K = K_x + iK_y$ the complex valued control amplitude. The mathematical properties of this nice model have been analysed in detail [5–7]. Without control, $K_x = K_y = 0$, the model possesses, in the sub-threshold regime $\lambda < 0$, the so-called Pyragas orbit

$$z_p(t) = R_p e^{i\Omega_p t}, \quad R_p = \sqrt{-\lambda}, \quad \Omega_p = 1 + \gamma R_p^2 \,. \tag{2}$$

Such an unstable orbit is of particular interest with regards of time delayed feedback control, as fundamental aspects of the noninvasive stabilisation can be studied when one meets a first-order Pyragas condition $\tau = 2\pi/\Omega_p$ for the delay time.

The model introduced by Fiedler et al. proposes a particular coupling scheme for the control force to allow for the stabilisation of the unstable state. Here we are concerned with the experimental implications of such a scheme. For that purpose we devise an experimental setup along the lines of the model Eq.(1). One may conjecture that our findings won't be

limited to our particular setup, as models like Eq.(1) are widely used and cover, for instance, typical oscillatory systems close to instabilities or simple single mode optical devices. To some extent our approach may be considered as an experimental bifurcation analysis, to uncover generic features of the control scheme devised along the lines of Pyragas, Schöll, and Fiedler. However, the main focus of our investigation is to prove whether the suggested coupling scheme can be successfully applied under realistic experimental conditions where, normally, mismatched or drifting parameters, insufficient sensitivity, and internal or external noise may severely limit the control performance.

II. EXPERIMENTAL SETUP

In order to realise an unstable periodic orbit without torsion we designed an autonomous electronic oscillator from active elements, i.e, operational amplifiers, adders, and multipliers. A diagrammatic view of our setup is shown in Fig.1. The two voltages U_x and U_y, both in the order of several volts, realise the real and imaginary parts of the oscillator state. The two circuits, indicated blue and yellow, generate the flow, and by integrating these output signals and feeding them back to the input we have two coupled closed loops. Their dynamics can be described by the coupled set of equations

$$\begin{aligned} U_x &= \int dt\, \omega_0(\lambda U_x - U_y) + \alpha(U_x^2 + U_y^2)(U_x - \gamma U_y) \\ U_y &= \int dt\, \omega_0(U_x + \lambda U_y) + \alpha(U_x^2 + U_y^2)(\gamma U_x + U_y)\,. \end{aligned} \tag{3}$$

The parameters of the circuit, $\omega_0 \approx 1.03 \cdot 10^3 \mathrm{s}^{-1}$, $\alpha \approx 120 \mathrm{s}^{-1}\mathrm{V}^{-2}$, $\lambda \approx -1.02$, and $\gamma \approx 10.0$ are determined by the combination of resistors in our setup. For further details of the experimental configuration see Ref.[8]. The correspondence between our setup and the normalised form of Eq.(1) can be achieved by rescaling time in units of ω_0^{-1} and all voltages in units of $(\omega_0/\alpha)^{1/2}$.

For defining the initial conditions of our experiment the integrator outputs can be set to adjustable constant voltages U_{x_0} and U_{y_0}, respectively. Switching on the system at $t = 0$, the variables $U_x(t)$ and $U_y(t)$ start from a well-defined state. When starting the uncontrolled system from initial conditions inside a range $U_R = (U_{x_0}^2 + U_{y_0}^2)^{1/2}$ of about 1.2V the system settles immediately in the stable fixed point at $U_x = U_y = 0$, while starting from outside this range the system escapes to the saturation limits of the operational amplifiers. The boundary

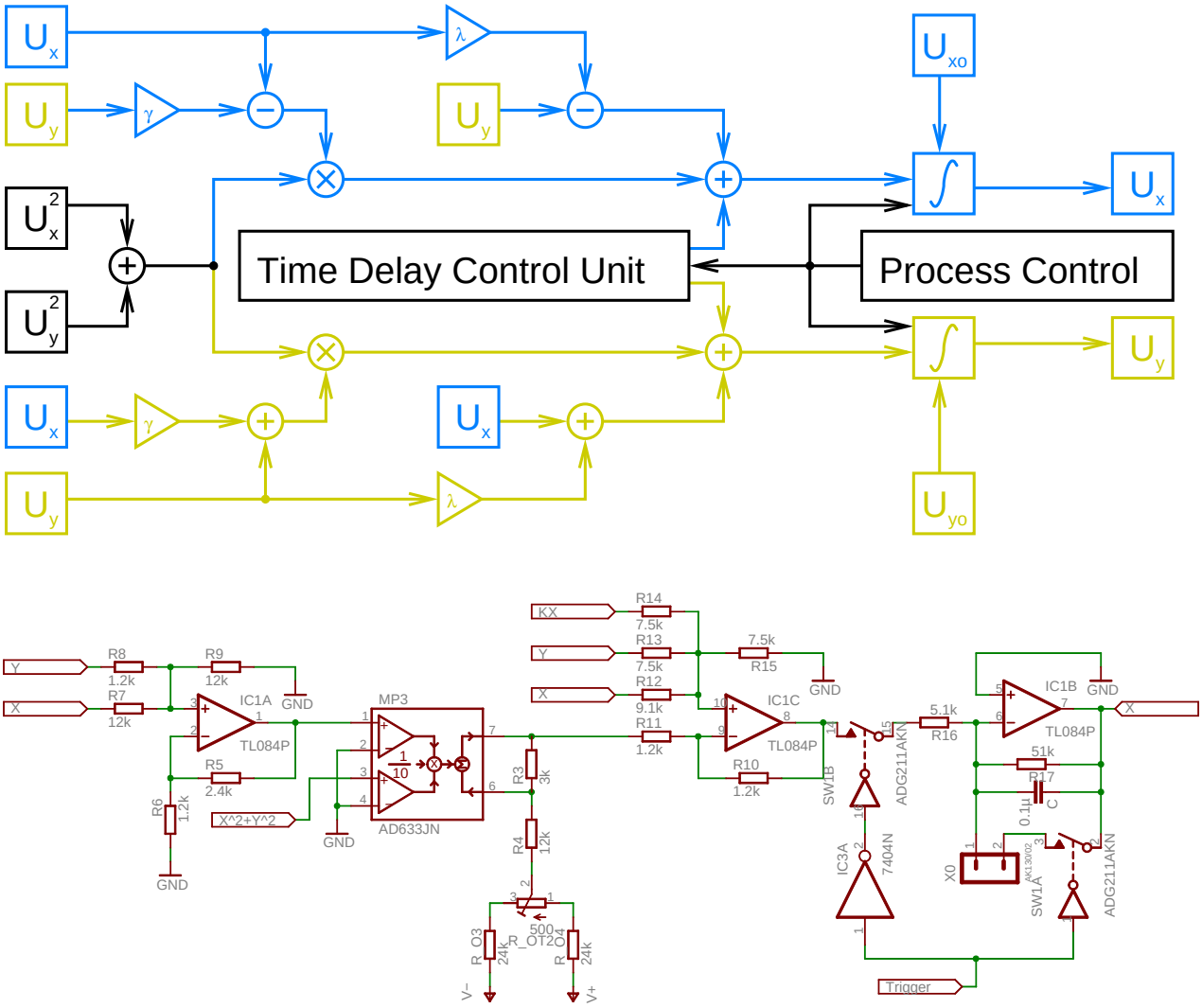

FIG. 1: (Color online) Top: Block diagram of the Stuart-Landau oscillator with control loop built from electronic components. Bottom: Actual design of one component (blue/medium) of the Stuart-Landau oscillator.

$U_R \approx 1.2$V limiting the basin of attraction of the fixed point indicates the position of the unstable orbit to be controlled.

The control scheme proposed in [5] was realised in the following way. The two components of the control voltage

$$\begin{aligned} F_x &= -K_x(U_x(t) - U_x(t-\tau)) + K_y(U_y(t) - U_y(t-\tau)) \\ F_y &= K_y(U_x(t) - U_x(t-\tau)) + K_x(U_y(t) - U_y(t-\tau)) \end{aligned} \tag{4}$$

are generated as illustrated in Fig.2. The input signals $U_x(t)$ and $U_y(t)$ are sent through separate digital delay lines to compose the control signals $U_{x,y}(t) - U_{x,y}(t-\tau)$. These voltages

are then multiplied by gain factors and mixed together in a way to form the intended coupling matrix of rotation type. The actual gains are determined by input voltages $U_{K,x}$ and $U_{K,y}$ at the input of operational amplifiers. These voltages are proportional to the normalised control amplitudes $\kappa_x = \tau K_x$ and $\kappa_y = \tau K_y$. In order to obtain well-defined delay signals the feedback loops generating the control signal are switched on at about one cycle after the oscillator. The setting of the system parameters, of delay time and control amplitudes, and the acquisition of data are handled by a separate module, allowing to run the whole experiment automatically.

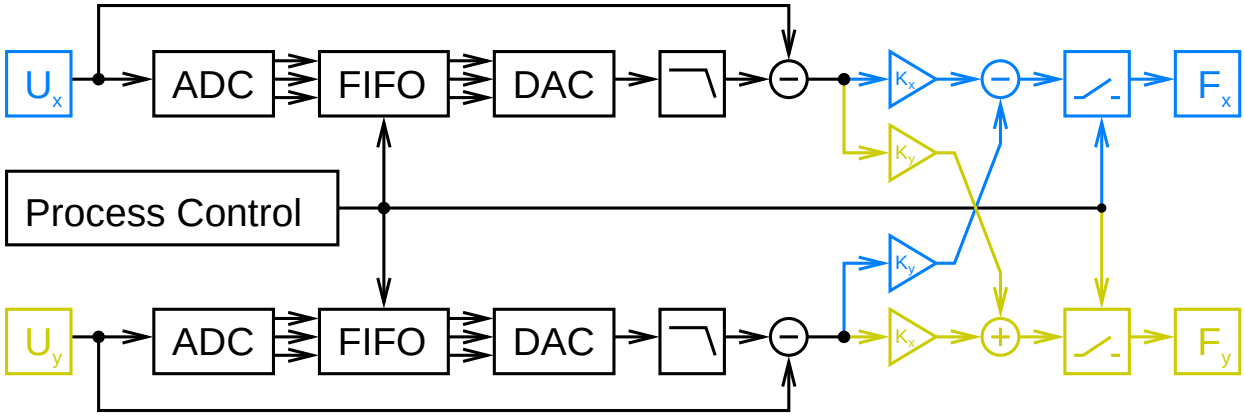

FIG. 2: (Color online) Design of the control loop based on two digital delay lines.

III. CONTROL PERFORMANCE AND DATA PROCESSING

Fig.3(a) demonstrates successful experimental implementation of Pyragas-Schöll-Fiedler control. For a large regime of the control amplitudes the Pyragas orbit can be stabilised, as indicated by regular periodic oscillations of the output voltages $U_x(t)$ and $U_y(t)$, and by almost vanishing control signals. The observed oscillation frequency of 1.92kHz deviates by less than 5% from the value $\nu = \omega_0 (1 - \gamma\lambda) / 2\pi \approx 1.84$ kHz calculated from circuit parameters. However, in spite of the symmetry of the setup the amplitudes of U_x and U_y differed by more than 10%, probably due to the effect of drifting multiplier offsets.

The successfully controlled Pyragas orbit can be clearly distinguished from control induced or quasiperiodic orbits which show up by pronounced oscillatory control signals of up to 0.5V in amplitude, Fig.3(c,d). In addition, it was quite straightforward to detect the fixed point (cf. Fig.3(b)).

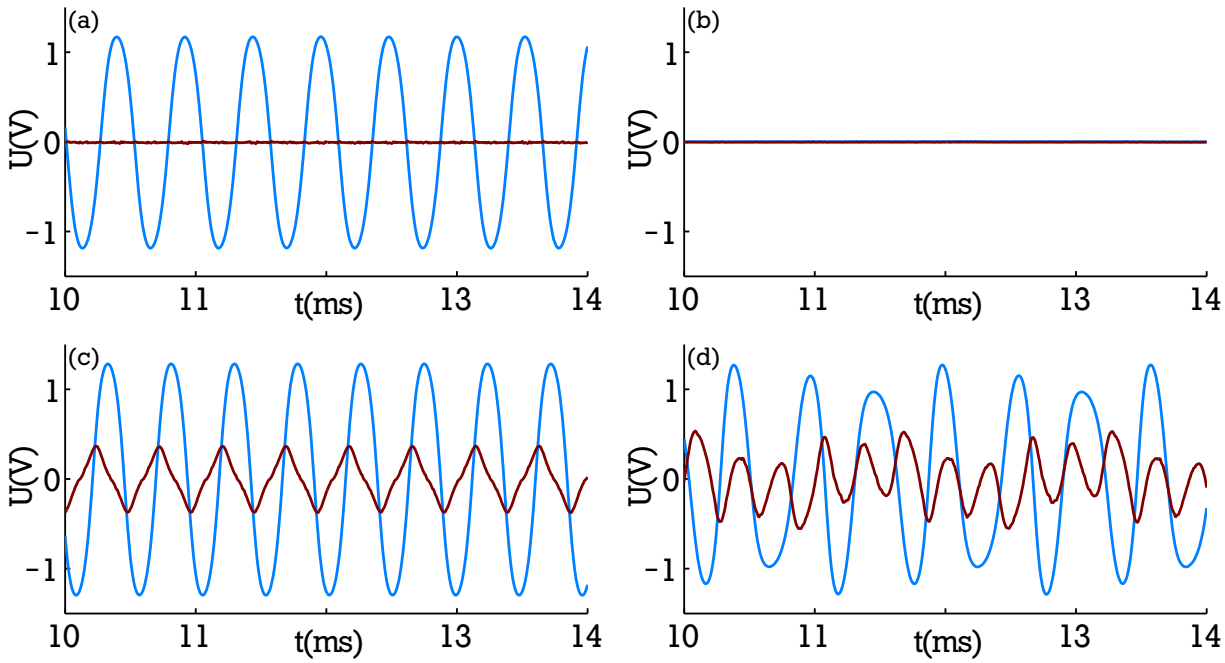

FIG. 3: (Color online) Time traces of the experimental circuit subjected to control (for a few typical values of the control gains $U_{K,x/y}$): (a) successful control of the Pyragas orbit, (b) trivial fixed point, (c) control induced periodic state, (d) control induced quasiperiodic state. Blue/medium: signal $U_x(t)$, red/dark: control voltage $F_x(t)$.

As our study will go far beyond a plain illustration of successful control, we require a reliable algorithm to detect attractors in experiments, e.g., the trivial fixed point, the Pyragas orbit, control induced periodic states, and torus solutions, to provide a comprehensive experimentally based bifurcation analysis including homoclinic bifurcations. For that purpose we use the Hilbert transforms of the output voltages and of the control forces to extract amplitudes of the signals. In that way a clear discrimination between different attractors and a reliable detection of bifurcations becomes possible. Fig.4 illustrates the successful measurement of a simple one-parameter bifurcation scenario.

We are now in a position to scan the control performance in the entire parameter plane. Fig.5 shows results for two different fixed initial conditions, i.e., a non-adiabatic parameter change. The control domain, i.e., the stabilised Pyragas orbit, as well as other attractors in neighbouring regimes are clearly detected. The dependence on initial conditions gives a hint of the shape of the basin of attraction in this high dimensional experimental setup [9]. These results verify by experimental means that Pyragas-Schöll-Fiedler control is a quite robust

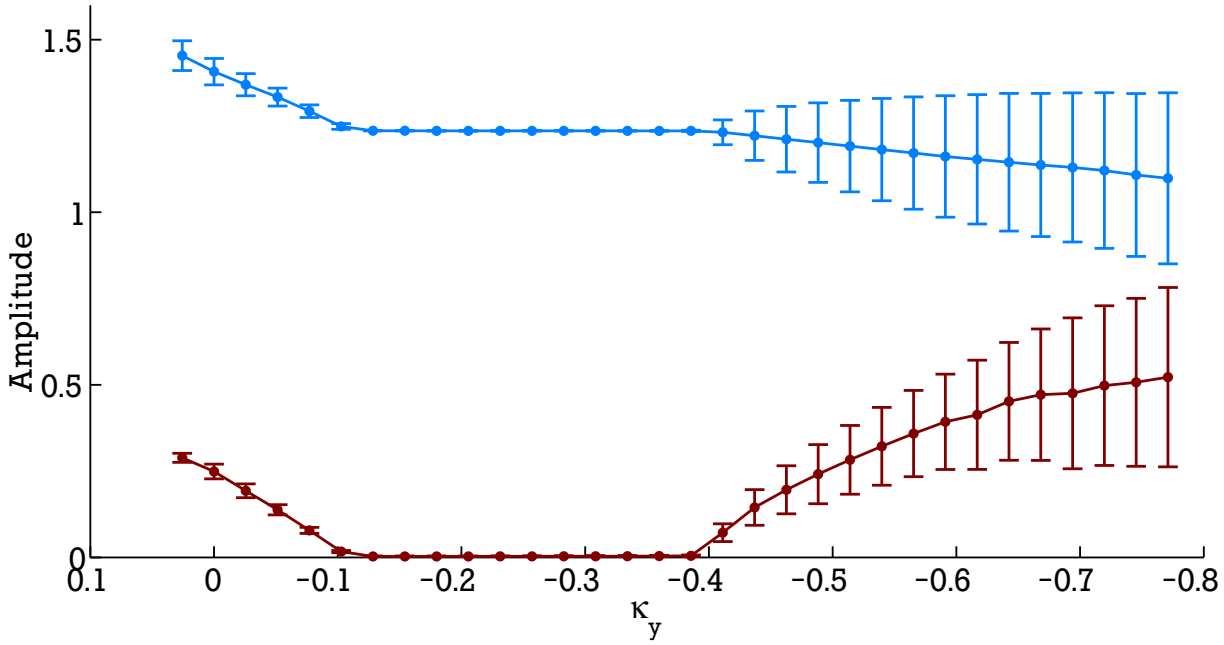

FIG. 4: (Color online) Mean value (line) and standard deviation (bars) of the amplitude (in volts) of of the signal U_x (blue/medium) and of the control force F_x (red/dark), as a function of the normalised control amplitude $\kappa_y = \tau K_y$ at $\kappa_x = \tau K_x = 0.265$ (corresponding to $U_{K,x} = 0.1$V). From left to right (i.e., increasing control amplitude in modulus): control induced periodic orbit followed by stabilised Pyragas orbit and quasiperiodic state.

method if parameters are chosen well inside the control domain, since successful control does not depend strongly on moderate noise and the choice of initial conditions.

IV. BIFURCATION ANALYSIS

To gain more insight into the shape of the control domain and into the mechanisms which limit the control performance, one may resort to a bifurcation analysis of the model (1). In principle such theoretical results can be found in the literature (cf., e.g., [6, 7]). However, to keep the presentation self-contained, to address the specific issues of our setup, in particular with regards to a quantitative comparison of experimental and theoretical results, and to set the notation used in the subsequent analysis, we briefly summarise the main features.

The condition for a general harmonic orbit $z_h(t) = R\exp(i\Omega t)$ is easily obtained from

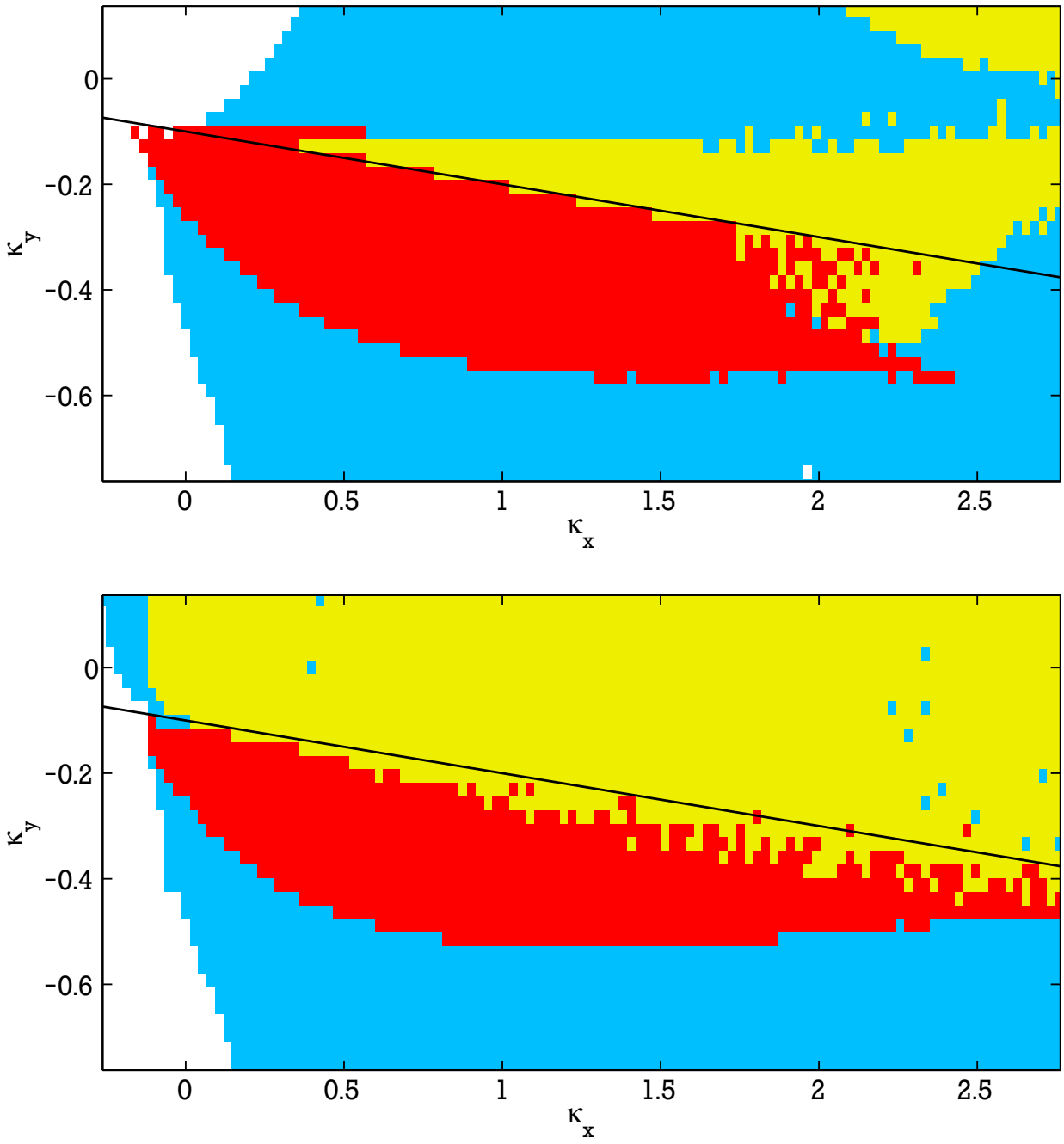

FIG. 5: (Color online) Experimentally recorded control performance for fixed initial condition. Top: initial voltage slightly larger than the Pyragas orbit ($U_R + 10\text{mV}$), bottom: initial voltage slightly smaller than the Pyragas orbit ($U_R - 20\text{mV}$). Red (dark): Pyragas orbit, yellow (light): trivial fixed point, blue (medium): control induced orbits, white: operational amplifiers saturate.

Eq.(1) as

$$i\Omega = \lambda + i + (1 + i\gamma)R^2 - (K_x + iK_y)(1 - e^{-i\Omega\tau}) \,. \tag{5}$$

Linear stability is determined by the variational equation which becomes autonomous if the analysis is carried out in a rotating frame because of rotational symmetry, $z(t) = z_h(t)(1 + \delta r(t) + i\delta\phi(t))$. Thus, one finally ends up with a characteristic quasi-polynomial

$$\begin{aligned} P(\mu, \omega, \rho^2) &= (1 - e^{-\mu})^2(\kappa_x^2 + \kappa_y^2) + \mu(-2\rho^2 + \mu) \\ &-2\rho^2(1 - e^{-\mu})[(\kappa_x + \gamma\kappa_y)\cos\omega + (\kappa_y - \gamma\kappa_x)\sin\omega] \\ &+2\mu(1 - e^{-\mu})(\kappa_x \cos\omega + \kappa_y \sin\omega) \end{aligned} \tag{6}$$

where we have used units rescaled by the time delay, i.e., $\omega = \Omega\tau$ for the frequency of the orbit, $\rho^2 = R^2\tau$ for its amplitude, and $\mu = \Lambda\tau$ for the Floquet exponent which is determined by the condition $P(\mu, \omega, \rho^2) = 0$. The rescaled control amplitudes $\kappa_{x/y} = \tau K_{x/y}$ are not mentioned explicitly in the list of arguments. As we are dealing with an autonomous system the Goldstone mode causes the root $\mu = 0$ of Eq.(6).

The κ_x-κ_y stability domain of the Pyragas orbit (2) with $\omega = 2\pi$ and $\rho^2 = -\lambda\tau$ is bounded by a transcritical and by a Hopf bifurcation. The transcritical line follows from a repeated root of Eq.(6), i.e., $\partial_\mu P(\mu = 0, 2\pi, -\lambda\tau) = 0$. The evaluation is straightforward and yields the line $\kappa_x = -1 - \gamma\kappa_y$. The other boundary of the control domain, i.e., the Hopf bifurcation line is easily obtained in parametric form by solving the bifurcation condition $P(\mu = i\varphi, 2\pi, -\lambda\tau) = 0$ for the two real valued control amplitudes, with the imaginary part of eigenvalue φ acting as the parameter of the curve.

The stability of the control induced orbits $z_h(t)$ can be evaluated along the same lines. The domain of existence is determined by saddle node bifurcations, i.e., via the condition $\partial_\mu P(\mu = 0, \omega, \rho^2) = 0$, or equivalently by a degenerate solution of Eq.(5). Again, a parametric representation of the boundary is easily constructed. At the transcritical line mentioned above, the Pyragas orbit $z_p(t)$ exchanges stability with such a particular control induced state. In addition, the stability region is bounded by a Hopf bifurcation and the corresponding condition, Eq.(5) and $P(\mu = i\varphi, \omega, \rho^2) = 0$, results straightforwardly in a rather involved expression.

Finally, the stability analysis of the trivial fixed point $z = 0$ determines a Hopf bifurcation line which, according to Eq.(1), is given by $i\varphi = \lambda\tau + i\tau - (\kappa_x + i\kappa_y)(1 - \exp(-i\varphi))$. With minimal further effort the type of bifurcation can be evaluated as well (cf., e.g., [6]).

The result of this simple partial bifurcation analysis is summarised in Fig.6 where all the features relevant for the control performance are indicated. The control domain of the Pyragas orbit and the stability domain of the control induced state causing the stability exchange are shaded. Among others, there are three higher-order codimension bifurcation points on the transcritical line which determine mainly the control performance. The leftmost point (TB) is a degenerate Takens-Bogdanov bifurcation where the Hopf bifurcations merge with the transcritical line. This point is determined by a triple root of the characteristic equation (6) and is given by $\kappa_y = [-\lambda\tau/(1+\gamma^2)]^{1/2}$. The right corner (TH) of the control domains is determined by the simultaneous intersection of the two Hopf boundaries with the transcritical line. Finally the extension of the stability region of the control induced state transverse to the transcritical line vanishes when the saddle node boundary touches the transcritical line causing a pitchfork bifurcation (P) at $\kappa_y = -\gamma/(1+\gamma^2)$.

To get a more intuitive understanding of the control performance let us consider on a smaller scale one-dimensional sections in the two-dimensional parameter plane close to the origin, where one changes the modulus $\kappa = (\kappa_x^2 + \kappa_y^2)^{1/2}$ and keeps the angle constant (cf. Fig.7). One clearly recognises how the Pyragas orbit with constant radius gains stability and how this mechanism interacts with the other bifurcations in the system.

V. STABILITY MEASUREMENTS

We prove that the experimental control properties match quantitatively the theoretical considerations. The measurement technique described in Sec.III allows the detection of bifurcations. For a detailed experimental analysis one requires a fairly low level of noise and, in particular, the ability to adjust the initial state in a reproducible way, in order to implement adiabatic parameter changes. Fig.8 summarises the results on the experimental control performance. The control domain is bounded by a transcritical line and by a Hopf bifurcation. The experimental results are in quantitative agreement with the theoretical model Eq.(1). All parameters of the model but one have been obtained from the experimental design. A constant amplification factor which enters the linear scaling between the voltages $U_{K,x/y}$ and the normalised control amplitudes $\kappa_{x/y}$ has been determined from the transcritical line. This boundary is quite suitable for calibration as a simple calculation following, e.g., the lines of [10] shows that the transcritical line is a straight line regardless of the underlying

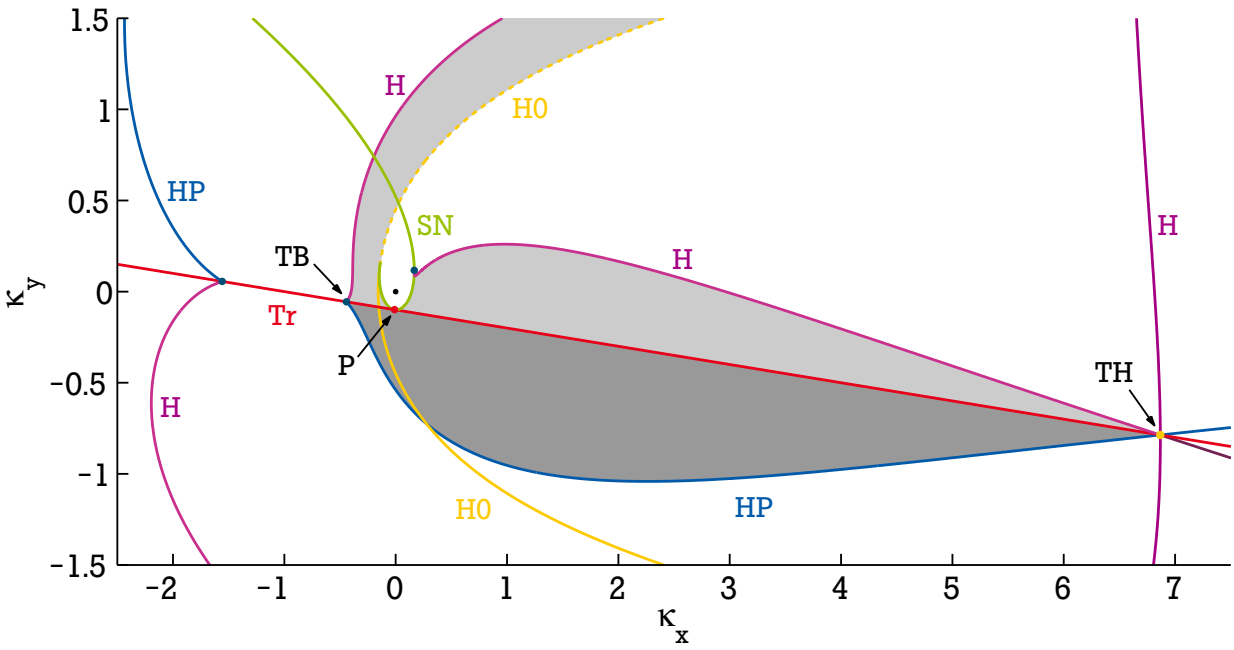

FIG. 6: (Color online) Partial bifurcation diagram of Eq.(1) for $\lambda = -0.1$ and $\gamma = 10$. Shaded: control domain of the Pyragas orbit (dark) and stability domain of the control induced state (light). Tr (red): transcritical bifurcation, HP (blue): Hopf bifurcation of the Pyragas orbit, SN (green): saddle node bifurcation of control induced harmonic solutions, H (violet): Hopf bifurcation of control induced solutions, H0 (yellow): Hopf bifurcation of the trivial fixed point (broken/solid: super-/subcritical bifurcation). Particular higher-order codimension points on the transcritical line: (TB) degenerate Takens-Bogdanov point, (TH) transcritical-Hopf bifurcation, (P) pitchfork bifurcation.

dynamics.

In addition, we traced not only those bifurcations limiting the control regime, but even more a variety of bifurcations related to the creation and annihilation of control-induced orbits or tori, which are also involved in the control mechanism. That includes the homoclinic bifurcation which is born in a Takens-Bogdanov bifurcation and which determines one of the stability boundaries of the quasiperiodic state. These secondary instabilities are again in quantitative agreement with the theoretical model, although slightly larger deviations are visible.

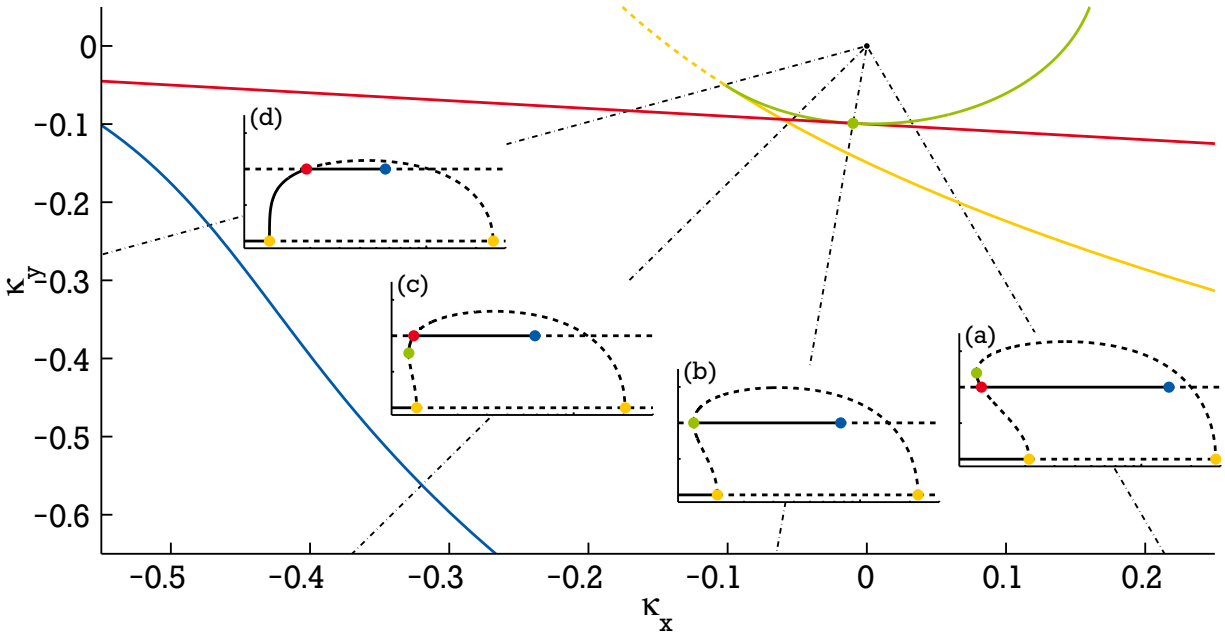

FIG. 7: (Color online) Control domain on a smaller scale (cf. Fig.6) for $\lambda = -0.03$, $\gamma = 10$ and bifurcation diagrams along particular one dimensional paths, illustrating in particular (a)/(c): transcritical bifurcation of the Pyragas orbit and subcritical Hopf bifurcation of the trivial fixed point, (b): pitchfork bifurcation of the Pyragas orbit and, (d): supercritical Hopf bifurcation of the trivial fixed point.

VI. CONCLUSION

We have presented, for the first time to our best knowledge, the successful implementation of Pyragas-Schöll-Fiedler control to stabilise torsion-free periodic orbits in autonomous dynamical systems. The experimental study which, in fact, constitutes an experimentally based bifurcation analysis of a system with time delay, is in striking quantitative agreement with analytical calculations. The analysis shows that the control scheme proposed on theoretical grounds is robust against imperfections which prevail in real world applications. In addition, and as expected from theoretical considerations, it has shown up to be vital that the orbit to be stabilised shows a substantial twist, i.e., a dependence of the period on the amplitude. Such twists may be either present in the system without control, or may be induced by the control loop. We think, the mechanisms which determine the control domain share quite a large degree of universality, as we have obtained comparable control

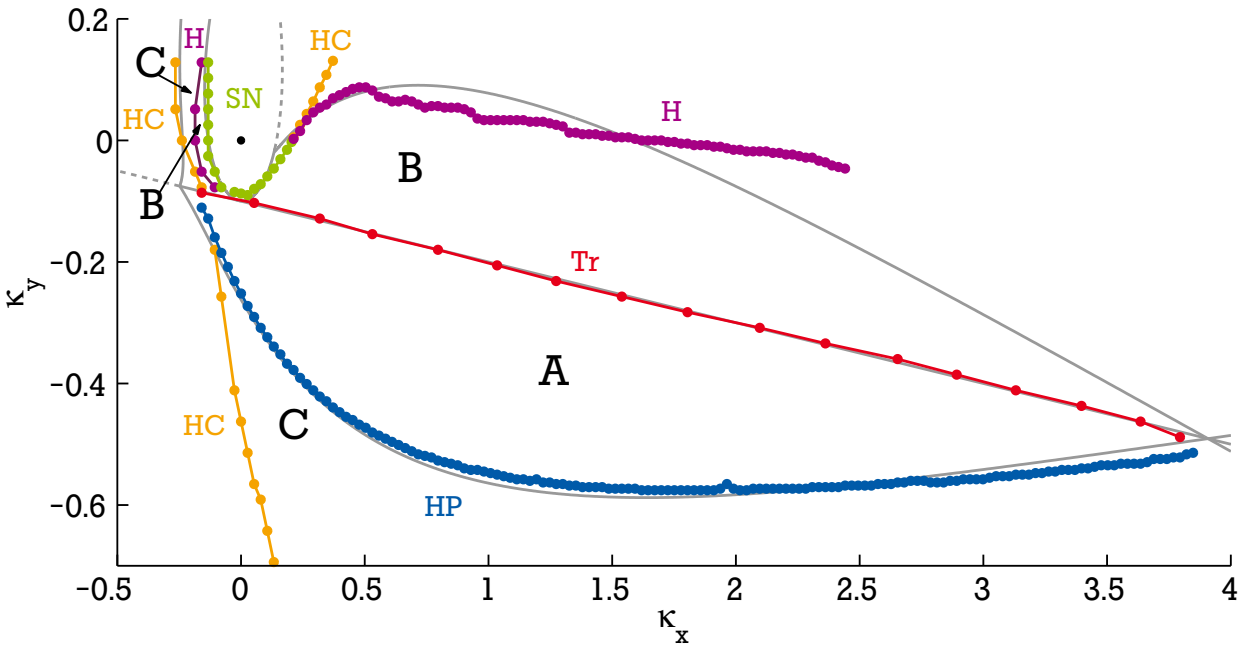

FIG. 8: (Color online) Control domains and instabilities measured in the electronic circuit experiment. Tr (red): transcritical bifurcation, HP (blue): Hopf bifurcation of the Pyragas orbit, SN (green): saddle node bifurcation of the control induced orbit, H (violet): Hopf bifurcation of the control induced orbit, HC (orange) homoclinic bifurcation of the quasiperiodic torus state. Control domain of the Pyragas orbit (A), stable domain of the control induced periodic state (B), stable domain of the torus state (C). Outside those regions the experiment either tends to the trivial fixed point or the amplifiers saturate, indicating an unbounded solution in the corresponding theoretical model. Lines are the results of the bifurcation analysis of the theoretical model (1) with parameters $\lambda = -1$ and $\gamma = 10$ (cf. Fig.6 as well).

performance with modified experimental setups. Furthermore, such a conjecture can be underpinned by recent general normal form calculations [11]. Thus, the results presented here can guide the implementation of time-delayed feedback control in diverse experimental setups such as lasers and other technologically relevant devices.

The focus of this study was mainly on experimental aspects of the control mechanism. It is, however, worth to mention that Eq.(1) allows for an almost complete analytical overview of all local bifurcations (cf. Fig.9) and reveals a quite nice regular structure. In fact, one can work out all Takens-Bogdanov points by analytical means. Such a result may provide vital input to compute all global bifurcations using continuation tools. In that respect the

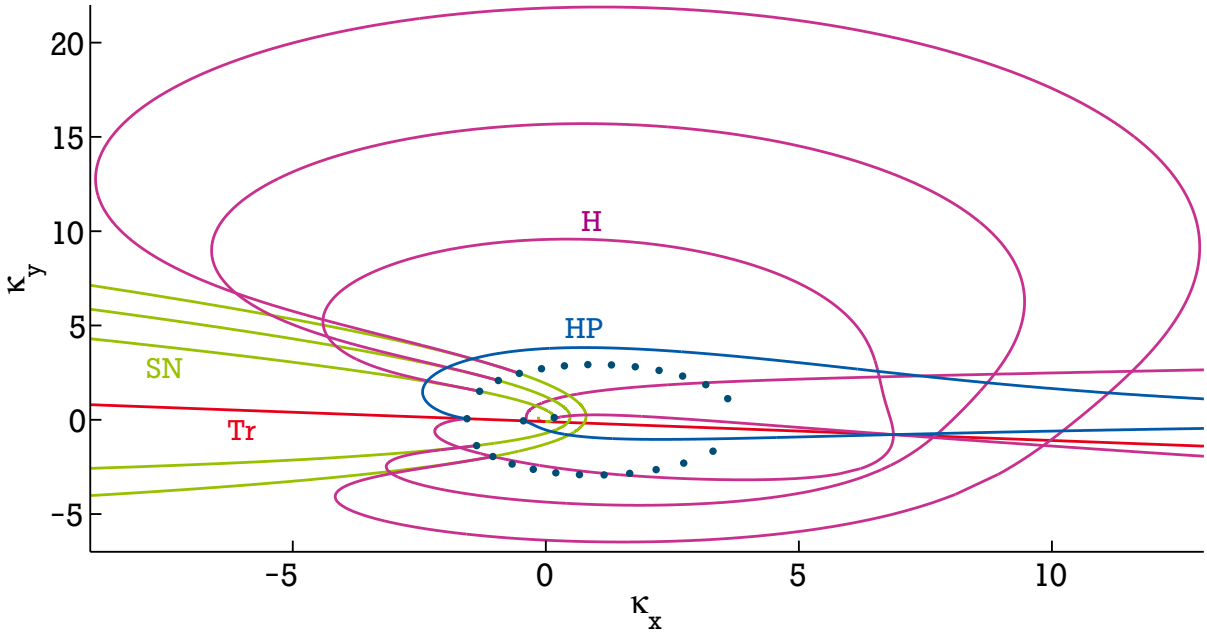

FIG. 9: (Color online) Partial bifurcation diagram of Eq.(1) for $\lambda = -0.1$ and $\gamma = 10$, showing all Takens-Bogdanov points. The related codimension-one Hopf (HP: blue and H: violet) and saddle node (SN: green) bifurcation lines show a distinct geometric structure which is organised by the circular array of codimension-two points. For clarity only a few bifurcation lines are shown.

model (1) seems to be one of the very few time delay systems where the complete set of higher-codimension bifurcation points is accessible. Based on such considerations one could even hope for a more detailed study of invariant manifolds, to clarify the basin of attraction of the Pyragas orbit, one of the major challenges for applications of time delayed feedback control.

---

[1] K. Pyragas, *Continuous control of chaos by self–controlling feedback*, Phys. Lett. A **170**, 421 (1992).

[2] *Handbook of Chaos Control (2nd edition)*, edited by E. Schöll and H. G. Schuster (Wiley-VCH, Weinheim, 2007).

[3] W. Just, A. Pelster, M. Schanz, and E. Schöll(Eds.), *Delayed complex systems*, Phil. Trans. Roy. Soc. A **368**, 301 (2010).

[4] H. Nakajima, *On analytical properties of delayed feedback control of chaos*, Phys. Lett. A **232**, 207 (1997).

[5] B. Fiedler, V. Flunkert, M. Georgi, P. Hövel, and E. Schöll, *Refuting the odd number limitation of time-delayed feedback control*, Phys. Rev. Lett. **98**, 114101 (2007).

[6] W. Just, B. Fiedler, M. Georgi, V. Flunkert, P. Hövel, and E. Schöll, *Beyond the odd number limitation: a bifurcation analysis of time-delayed feedback control*, Phys. Rev. E **76**, 026210 (2007).

[7] H. Erzgräber and W. Just, *Global view on a generic nonlinear oscillator subject to time-delayed feedback control*, Physica D **238**, 1680 (2009).

[8] C. von Loewenich, *Controlling torsion-free periodic orbits by time-delayed feedback control*, Ph.D. thesis, TU Darmstadt, 2010 (url: http://tuprints.ulb.tu-darmstadt.de/2083).

[9] K. Yamasue and T. Hikihara, *Domain of attraction for stabilized orbits in time delayed feedback controlled Duffing systems*, Phys. Rev. E **69**, 056209 (2004).

[10] W. Just, H. Benner, and C. von Loewenich, *On global properties of time-delayed feedback control: weakly nonlinear analysis*, Physica D **199**, 33 (2004).

[11] G. Brown, C. M. Postlethwaite, and M. Silber, *Time-delayed feedback control of unstable periodic orbits near a subcritical Hopf bifurcation*, preprint arXiv:1006.3479v1 (2010).